Nanoscale Advances

ROYAL SOCIETY OF CHEMISTRY

PAPER

View Article Online
View Journal | View Issue



Cite this: *Nanoscale Adv.*, 2024, **6**, 146

# Correlating structural changes in thermoresponsive hydrogels to the optical response of embedded plasmonic nanoparticles†

Kamila Zygadlo,[a] Chung-Hao Liu,[b] Emmanuel Reynoso Bernardo,[a] Huayue Ai,[a] Mu-Ping Nieh[bc] and Lindsey A. Hanson*[a]

Stimuli-responsive microgels, composed of small beads with soft, deformable polymer networks swollen through a combination of synthetic control over the polymer and its interaction with water, form a versatile platform for development of multifunctional and biocompatible sensors. The interfacial structural variation of such materials at a nanometer length scale is essential to their function, but not yet fully comprehended. Here, we take advantage of the plasmonic response of a gold nanorod embedded in a thermoresponsive microgel (AuNR@PNIPMAm) to monitor structural changes in the hydrogel directly near the nanorod surface. By direct comparison of the plasmon response against measurements of the hydrogel structure from dynamic light scattering and nuclear magnetic resonance, we find that the microgel shell of batch-polymerized AuNR@PNIPMAm exhibits a heterogeneous volume phase transition reflected by different onset temperatures for changes in the hydrodyanmic radius ($R_H$) and plasmon resonance, respectively. The new approach of contrasting plasmonic response (a measure of local surface hydrogel structure) with $R_H$ and relaxation times paves a new path to gain valuable insight for the design of plasmonic sensors based on stimuli-responsive hydrogels.

Received 9th September 2023
Accepted 15th November 2023

DOI: 10.1039/d3na00758h

rsc.li/nanoscale-advances



## Introduction

Stimuli-responsive hydrogels are soft, deformable polymer networks that swell with water in response to a physical or chemical stimulus. Due to the extensive development of synthetic control over the properties of the polymer and its interaction with water, it has been reported that hydrogels can swell or collapse in response to light, temperature, electric field, pH, and specific chemicals.[1,2] In addition, size control of micro- or nanogels affords the possibility of delivery in confined spaces, as is the case for intravenous drug delivery,[3] and can change the cellular response in the case of synthetic extracellular matrices.[4] Small size also allows for faster responses, with the timescale of the volume phase transition scaling with the square of the radius of the particle, according to the Tanaka model.[5] Microgels also offer the possibility for synthetic control over complex architectures,[6] such as core–shell or core–shell–shell spheres that allow for response to multiple stimuli[7] or tune the kinetics of the volume phase transition.[8] This tunability and functionality make stimuli-responsive hydrogels promising materials for a variety of applications, from targeted drug delivery[2] to adaptable catalysis,[9] but a deeper understanding of their structures and responses to stimuli, especially at small length scales, is needed to fully take advantage of their potential.

Thermoresponsive gels are among the most well-studied stimuli-responsive hydrogels in the literature.[10–12] Thermoresponsive gels generally respond to temperature changes by undergoing a volume phase transition at a critical transition temperature, due to a change in the solubility of the polymer in water at that temperature. The prototypical thermoresponsive hydrogels are poly(*N*-isopropylacrylamide) (PNIPAm) and the closely related poly(*N*-isopropylmethacrylamide) (PNIPMAm), both of which undergo a volume phase transition at elevated temperatures due to desolvation of the hydrophobic isopropyl groups.[10] As a result, the hydrogels exhibit a decrease in volume above the critical solution temperature. The volume change serves as the origin of many applications of thermoresponsive hydrogels, including smart windows[11] and tunable photonic crystals.[12]

One particular complex architecture of interest is the combination of stimuli-responsive microgels with inorganic nanoparticles.[13] In particular, metallic nanoparticles exhibit localized surface plasmon resonances (LSPR) that yield strong absorbance and scattering features in the visible and near-

[a]*Department of Chemistry, Trinity College, Hartford, CT 06106, USA. E-mail: lindsey.hanson@trincoll.edu*

[b]*Polymer Program, Institute of Materials Science, University of Connecticut, Storrs, CT 06269, USA*

[c]*Chemical & Biomolecular Engineering Department, University of Connecticut, Storrs, CT 06269, USA*

† Electronic supplementary information (ESI) available: Additional electron microscopy, optical spectroscopy, NMR and SAXS measurements (PDF). See DOI: https://doi.org/10.1039/d3na00758h

infrared spectra. These resonances depend on the size and shape of the particle, as well as the refractive index at the surface of the particle.[14,15] Previous work has established the ability to synthesize microgels with metallic nanoparticles adsorbed to the exterior,[16–20] formed *in situ* in the microgel,[9] or embedded in the interior and used to seed the polymerization.[21] The composites add the advantage of the sensitive, strong optical response of the nanoparticles to the stimulus response of the hydrogel. The heat generated by the nanoparticle plasmon has been shown to initiate collapse of the hydrogel[19,22] to form a photoresponsive composite, and other work has shown that collapse of the gel reversibly alters the optical extinction of the composite[23] and tunes the plasmon resonance of the nanoparticle[24,25] to create devices with temperature-controlled optical absorbance. This latter work establishes the ability of the nanoparticle plasmon spectrum to report the state of the hydrogel, but to date this ability has not been leveraged to study the gel itself.

Here, we synthesize gold nanorods (AuNRs) embedded in a thermoresponsive PNIPMAm microgel and take advantage of the sensitive plasmon resonance to study the spatial heterogeneity of the thermoresponse of the newly formed AuNR@PNIPMAm microgels at various temperatures. As expected, the thermoresponsive hydrogel exhibits a thermally-induced collapse that is accompanied by an increase in the refractive index due to decreased water content.[26] The gold nanorod plasmon resonance red-shifts in response to the increase in refractive index and as such detects the degree of collapse at the surface of the nanorod. However, by contrasting dynamic light scattering (DLS) and nuclear magnetic resonance (NMR) measurements of the hydrogel with the plasmon response, we are able to differentiate between the degree of collapse at the nanorod surface with that in the rest of the microgel. This combined approach, to our knowledge the first of its kind to apply these three techniques together to such systems, allows us to provide insight into the variation in the volume phase transition throughout the microgel and provides a platform for future studies on the structure of stimuli-responsive nanocomposites.

## Results and discussion

In order to form AuNR@PNIPMAm microgels, AuNRs were first synthesized and then a thermoresponsive hydrogel was grown from the surface of AuNRs. AuNRs with mixed ligand shells of hexadecyltrimethylammonium bromide (CTAB) and sodium oleate (NaOL) were synthesized according to previously reported procedures.[27] Transmission electron microscopy (TEM) of a typical batch of as-synthesized AuNRs (Fig. S1†) confirmed the uniformity in size and shape with an aspect ratio of ~3.5, although the aspect ratio varies between 2.5 and 4 for different batches. We then measured their extinction spectra in varying concentrations of glycerol (Fig. S2†) to determine the sensitivity of each batch of nanorods to refractive index. The extinction spectra of the nanorods in water exhibit two resonances that correspond to the transverse plasmon resonance in the visible (around 515 nm) and the longitudinal resonance in the near-infrared (around 890 nm). In various batches of nano rods, longitudinal resonance varies between 800 and 900 nm as aspect ratio varies. Both resonances shift to longer wavelengths with increasing refractive index, but the longitudinal plasmon resonance is noticeably more sensitive, with a refractive index sensitivity of 310 nm per refractive index unit (Fig. S2†). That sensitivity varies with aspect ratio, and we have measured it between 230 and 320 nm per RIU for various batches. This range of sensitivities is in line with previous reports of refractive index sensitivity of high aspect ratio gold nanorods.[15]

The microgel grows from the nanorod surface by seeded polymerization[28] after partial ligand exchange for a polymerizable ligand, *N*,*N*′-bis(acryloyl)cystamine (BAC). Both plasmon resonances blue shifted slightly after ligand exchange, but there was no apparent change in AuNR morphology by TEM (Fig. S1†). The microgel was grown by seeded batch precipitation polymerization with a 10 : 1 ratio of the monomer, *N*-isopropylmethacrylamide, to the crosslinker, *N*,*N*′-methylenebis(acrylamide), by weight. The polymerization was performed above the lower critical solution temperature (LCST) of the NIPMAm to induce precipitation,[29,30] and thus the solution appeared cloudy during the synthesis. When cooled to room temperature, the newly grown microgels swelled with water and there was a marked decrease in the scattering by the polymer. The plasmon resonance red-shifted slightly after growth of the microgel due to the change in the refractive index at the surface (Fig. S3†).

Grid stained TEM (Fig. 1b) confirmed the formation of AuNR@PNIPMAm beads, which appear darker than the surrounding support film due to accumulation of phosphotungstic acid stain both at the surface and throughout the microgel. The boundary of the microgel appears darker than the interior, typical of a negative stain that accumulates at the edge of the particle as it dries. This is consistent with previously observed staining of similar microgels.[31] Notably, all of the nano rods observed are encapsulated by microgels, with only one nanorod per bead. However, in a typical synthesis there was a substantial number of PNIPMAm microgels that nucleated separately from any nanorods and appear empty. These empty microgels have lower mass than the AuNR@PNIPMAm microgels and can be removed by repeated centrifugation.

Upon heating the AuNR@PNIPMAm beads above their LCST, PNIPMAm undergoes a rapid volume-phase transition caused by water expulsion from the polymer.[32,33] This change in water content causes an increase in the refractive index of the hydrogel,[22,26] which in turn causes a red shift in the AuNR plasmon resonance. A representative set of extinction spectra of AuNR@PNIPMAm beads between 10 °C and 80 °C are shown in Fig. 1c. A red shift in the plasmon was observed with increasing temperature, which is most rapid at a transition temperature of 45 °C (Fig. 1d), corresponding to the LCST. A single, sharp transition is observed, similar to that observed in optical transmittance of AuNR coated with PNIPAm in previous work.[23] This behavior was not observed in AuNRs in the absence of PNIPMAm (Fig. S4†). It should be noted that the transition examined here was induced by bath heating and not due to plasmon excitation, as the power density in the

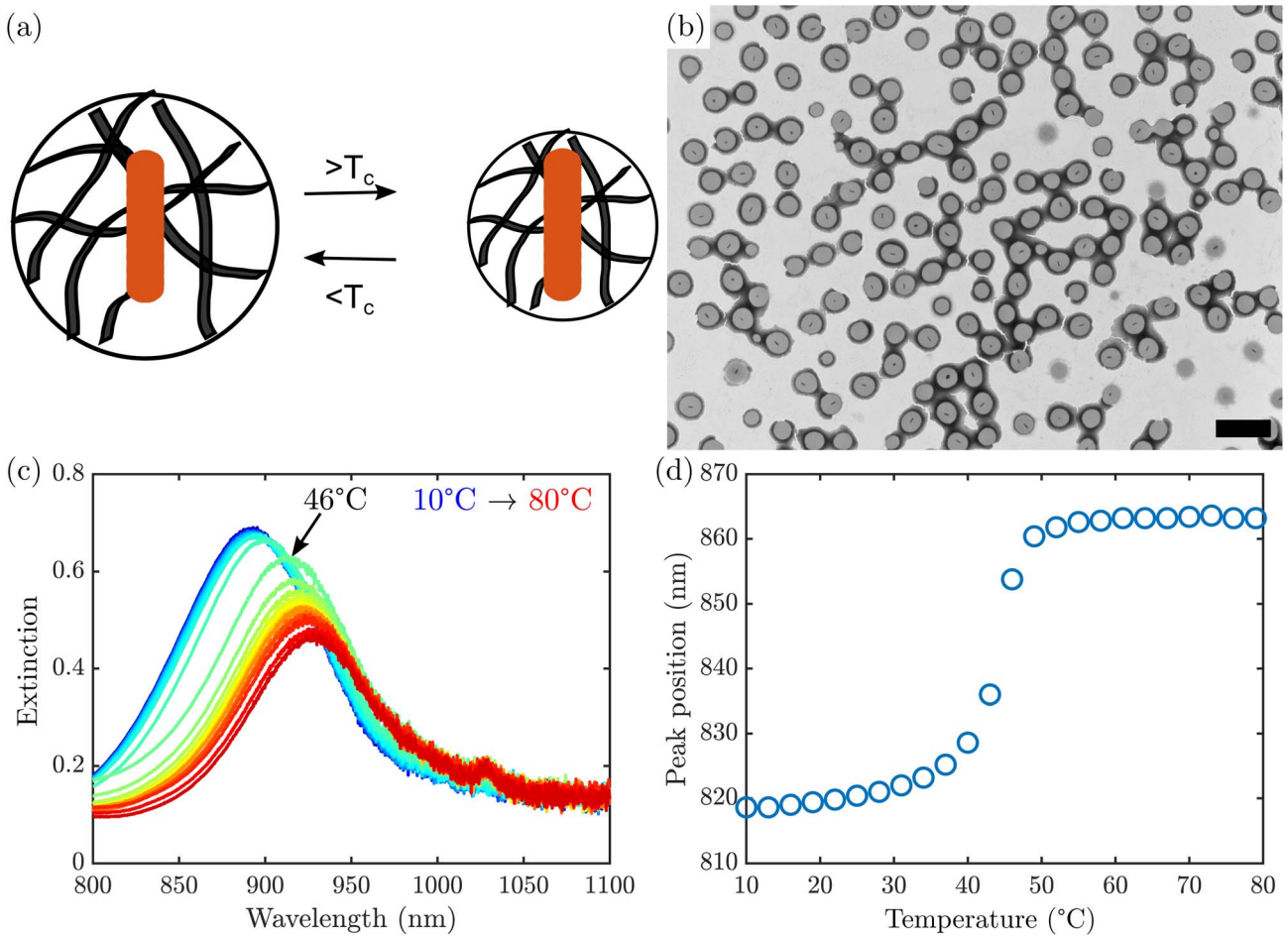


Fig. 1 Synthesis and characterization of AuNR@PNIPMAm microgels. (a) Schematic of volume phase transition in AuNR@PNIPMAm microgels. (b) TEM micrograph of AuNRs embedded in poly(*N*-isopropylmethacrylamide) (PNIPMAm) microgel. The scalebar is 500 nm. (c) NIR extinction spectra of AuNR@PNIPMAm in solution, taken every 3 °C between 10 °C and 79 °C. A large shift is seen between the spectra indicated at 43 and 46 °C. (d) Longitudinal plasmon peak position *versus* temperature. A rapid red-shift is observed around the phase transition temperature.

spectrophotometer is several orders of magnitude below the minimum threshold seen in studies with near-infrared laser excitation.[22]

The position of the plasmon resonance can be combined with refractive index calibration of the nanorods to determine the degree of collapse of the gel. In our measurements, the final peak position corresponds to a refractive index of 1.54, in agreement with previous reports of the refractive index of dry PNIPMAm or PNIPAm in the bulk.[34,35] However, earlier light scattering studies found a lower refractive index of PNIPMAm microgels above the LCST, implying incomplete collapse.[36] We propose that the difference is due to the plasmon measurement providing a more accurate depiction of the core of the bead, as the plasmon is most sensitive to the environment within the first few nanometers of the surface of the nanoparticle,[37] whereas light scattering measures the properties of the entire gel particle. As established by neutron scattering measurements,[38,39] microgels synthesized by batch polymerization such as the ones used in our experiment are more densely crosslinked near the center of the particle than at the surface. This supports the hypothesis that there would be a higher degree of collapse near the center of the bead, closest to the nanoparticle, than in the exterior of the particle. The effect of such structural heterogeneity on the collapse process, however, has not been previously reported and was only possible by direct comparison of the techniques presented here.

In order to further elucidate how the optical response of the nanorod corresponds to the degree of collapse in the bulk of the hydrogel, we examined the hydrodynamic radius of the AuNR@PNIPMAm microgels by DLS and diffusion-ordered nuclear magnetic resonance spectroscopy (DOSY NMR). At 298 K, DLS of the AuNR@PNIPMAm microgels [Fig. S5†] show a fully swollen gel at room $T$ with a hydrodynamic radius, $R_H$, that varies between samples, ranging between 200 and 450 nm. This agrees with the one-dimensional $^1$H NMR of the AuNR@PNIPMAm showing four peaks between 0 and 4.5 ppm that are broadened by the slow diffusion of the large bead (Fig. S8†) corresponding to the backbone and sidechain protons of the PNIPMAm and the crosslinker. In DOSY NMR, the integration of the backbone and sidechain peaks shows two

components (Fig. 2a), including a faster-diffusing signal due to trace small molecules and a slower-diffusing component with a diffusion constant of $8.5 \times 10^{-13}$ m$^2$ s$^{-1}$. The slowly diffusing component corresponds to a hydrodynamic radius of 480 nm as calculated by the Stokes–Einstein equation,[40] in good agreement with the hydrodynamic radius measured by DLS.

The $R_H$ of the microgel exhibits a transition of large hysteresis over a temperature range between 30 and 47 °C, at which the plasmon resonance has a red shift. The transitions of $R_H$ take place at ~30 °C upon heating and at ~47 °C upon cooling. In contrast, the plasmon response shows a much narrower hysteresis under thermal cycle (Fig. 2c). Comparison of the plasmon resonance and the $R_H$ response of the same sample upon heating suggests that the sudden decrease of $R_H$ at 30 °C does not exactly correlate to the optical response of the AuNR plasmon (Fig. 2d). Similar temperature-dependent structural transformation was observed in both repeated syntheses of AuNR@PNIPMAm (Fig. S6†) as well as in PNIPMAm microgels in the absence of AuNRs (Fig. S7†). This consistent discrepancy between the onset of size change of the microgel and that of the plasmon resonance transition suggests that the collapse of PNIPMAm upon heating takes place initially at the more loosely crosslinked exterior region of the shell. The transition then propagates to the interior at higher temperature until the collapse of the more densely crosslinked core near the surface of the AuNR leads to the transition of the plasmon resonance, which is sensitive to the dielectric environment within a few nanometers of the surface of the AuNR. Here, it should be noted that small angle X-ray scattering (SAXS) patterns from the AuNR@PNIPMAm at different temperatures stay invariant

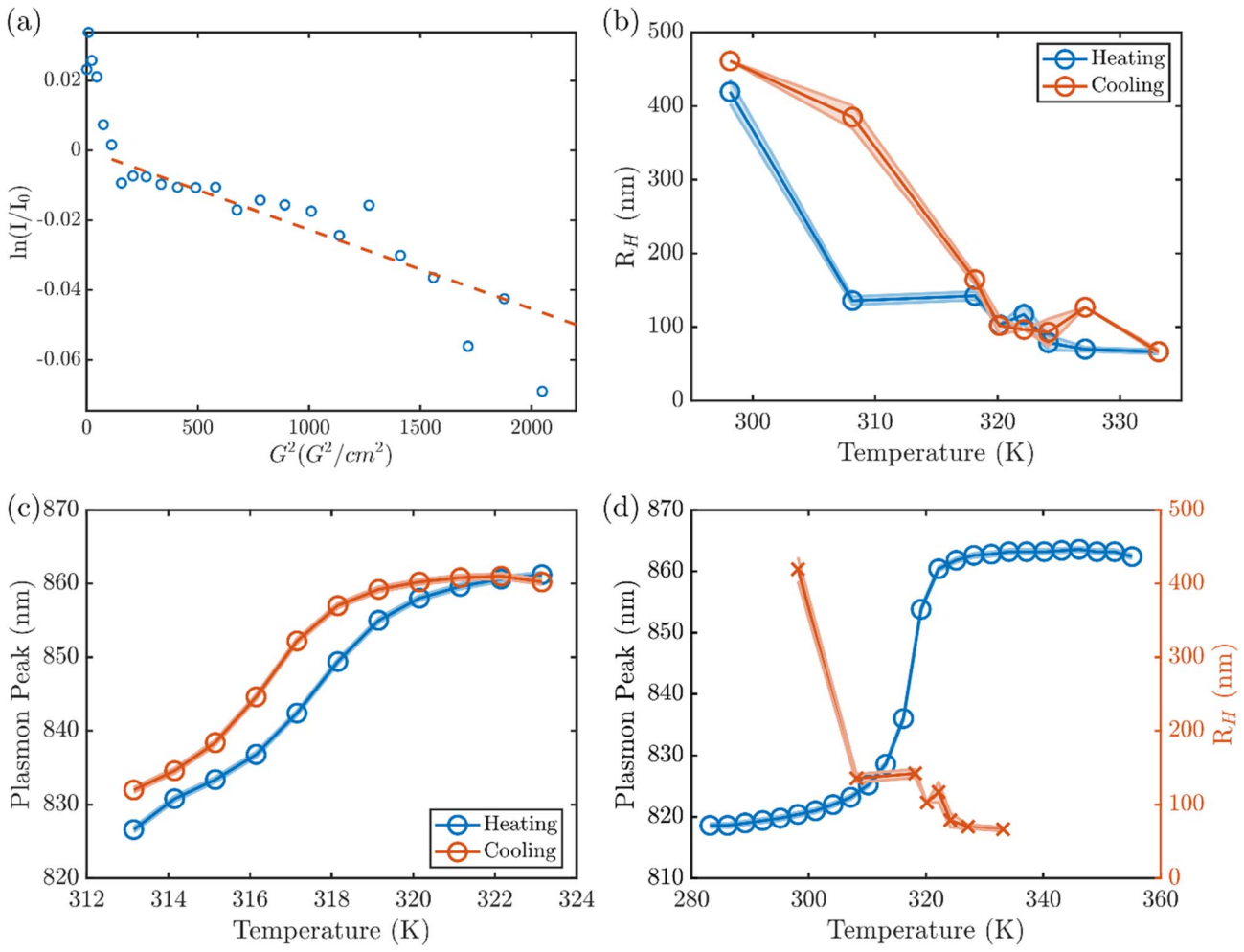


Fig. 2 Temperature-dependent behavior of AuNR@PNIPMAm microgels. (a) Diffusion-ordered NMR spectroscopy of the PNIPMAm backbone protons. A biexponential decay of intensity with the square of the gradient strength indicates two different diffusion constants, where the slowly diffusing component that corresponds to the hydrodynamic radius of the microgel. (b) Dynamic light scattering measurements of the hydrodynamic radius of AuNR@PNIPMAm microgels while increasing and decreasing temperature. Two transitions are seen, with significant hysteresis between heating and cooling. Shaded regions indicate uncertainty determined from repeated measurements. (c) Longitudinal plasmon peak position while increasing and decreasing temperature shows a single transition with hysteresis of only 1 °C. Shaded regions indicate uncertainty determined from repeated measurements. (d) Longitudinal plasmon peak position (left *y*-axis, circles) and hydrodynamic radius (righthand *y*-axis, x marks) *vs.* temperature of the sample AuNR@PNIPMAm sample. Shaded regions indicate uncertainty determined from repeated measurements.

during both heating and cooling (Fig. S9†), suggesting there is no temperature-dependent structural variation (*e.g.*, coalescence or aggregation) of the AuNR core.

In addition to the $R_H$ of the microgels obtained from DLS and DOSY NMR, the NMR spin-lattice (T1) relaxation time also reveals the solvation environment of the PNIPMAm,[41] providing molecular insight into the collapse of the hydrogel at various temperatures. The average T1 relaxation time of the protons attributed to the PNIPMAm backbone exhibits a non-monotonic dependence on temperature, with an initial decrease between 298 and 303 K followed by a larger increase between 313 and 316 K (Fig. 3a). However, the spin-lattice relaxation of the hydrogel protons is not always well described by a single exponential, as typically seen when measuring a uniform population of protons. This can be first seen by the large uncertainties in the T1 times determined by a monoexponential fit to the recovery at 298 K and 316 K. On the other hand, the relaxation time of the faster of two components in a biexponential fit shows a much smaller uncertainty (Fig. 3a). For closer inspection, the integrated area of the backbone proton peak at 1.9 ppm *versus* delay time in the inversion recovery NMR experiment at various temperatures are shown in Fig. 3b–d. At 298 K, a least-squares fit of the recovery to a single exponential function yields clear discrepancies between the data and the fit (Fig. 3b), and two different exponential components are needed to reproduce the relaxation behavior. (The results of mono- and biexponential fits to the data, along with their 95% confidence intervals, are shown for all temperatures in Fig. S10.†) This heterogeneity in relaxation is consistent with the expected heterogeneity of these hydrogels.

With a small increase in temperature to 303 K, however, the heterogeneous environment of the hydrogel backbone appears to be altered. The recovery converges to a single exponential component (Fig. 3c), indicating a uniform solvation environment and mobility of the backbone at that temperature. With further increasing temperature, the monoexponential recovery is maintained through 313 K (Fig. S10†), but at 316 K a long-lived component reemerges (Fig. 3d) that corresponds to the beginning of the volume phase transition throughout the gel.

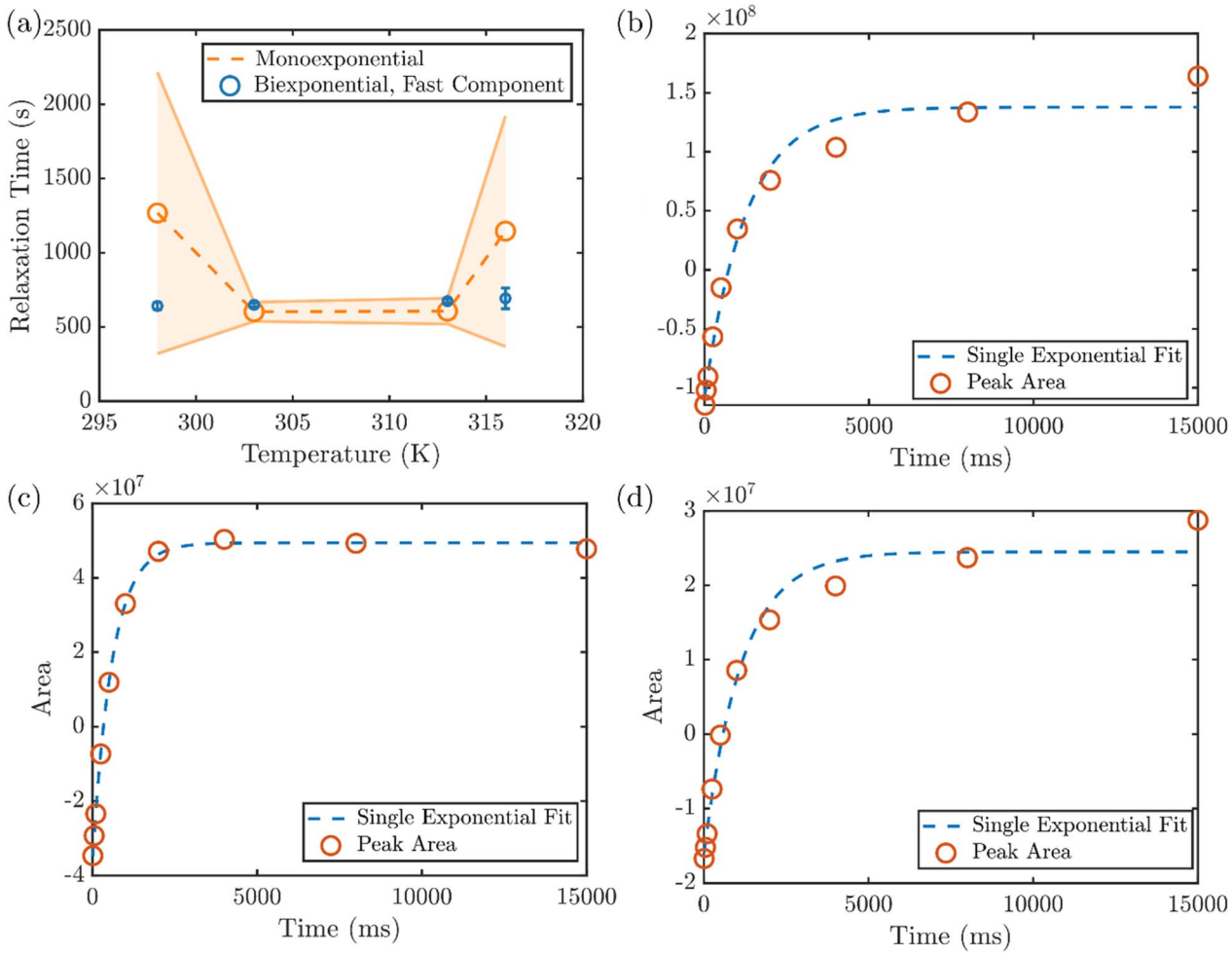


Fig. 3 NMR T1 Relaxation of AuNR@PNIPMAm microgels. (a) Inversion recovery times of PNIPMAm protons *versus* temperature. After fitting with a single exponential (orange, 95% confidence shown as shaded region) two transitions are seen, first between 298 and 303 K and another between 313 and 316 K. The shorter lifetime component of a biexponential fit is shown in blue. (b–d) Inversion recovery of the backbone proton of PNIPMAm in AuNR@PNIPMAm at 298 K (b), 303 K (c), and 316 K (d). A non-monoexponential inversion recovery is seen at 298 K and 316 K, while at 303 K, recovery is monoexponential.

Above that temperature, the full collapse of the hydrogel prohibits measurement by solution NMR. This two-stage change in the solvation environment of the PNIPMAm, to our knowledge not previously reported, is consistent with the two temperatures at which the initial reduction of $R_H$ is observed in DLS, corresponding to the collapse of the exterior of the hydrogel shell, at a temperature below the LCST (~30 °C) and the shift onset of the plasmon resonance, attributed to the collapse of the interior of the microgel, at the LCST (~47 °C).

By comparing the localized plasmon measurement to the overall change in volume of the bead, we can establish how the degree of collapse varies across the particle. Below 298 K, AuNR@PNIPMAm are fully solvated and exhibit similar plasmon resonance peak wavelengths to the as-synthesized AuNRs. However, with increasing temperature (~303 K), the heterogeneously crosslinked AuNR@PNIPMAm exhibit a volume phase transition, where $R_H$ starts to decrease from the exterior region. The onset of hydrodynamic collapse is accompanied by a partial change in solvation of the PNIPMAm backbone as seen in T1 NMR, but no change in plasmon resonance. This newly identified disconnect indicates that the transition begins in the exterior of the microgel, and that there is a substantial physical change in the hydrogel which is not sensed by the AuNR plasmon. Upon further increase in temperature the PNIPMAm completely collapses at ~320 K, and it is only the completion of the transition leads to the red-shift of the plasmon resonance. This set of unique insights into the thermoresponse of this system was only made possible by the new combination of all three techniques applied here.

Here we have shown that the crosslinked AuNR@PNIPMAm particles are not only heterogeneous in their structure at ambient temperature, but also heterogeneous during collapse at higher temperature. With increasing interest in plasmonic composites with stimuli-responsive hydrogels as a path toward multifunctional sensors, it is vital to understand how the embedded plasmonic nanoparticle responds to environment in the presence of surrounding hydrogel. While previous work has focused on the agreement between the hydrodynamic radius and the plasmon response, the regimes of disagreement are equally important to the overall performance of these composite sensors. By combining careful examination of three independent measures of sensor response, we gained new insight into the role of structural homogeneity in the functionality of a prototypical thermoresponsive sensor. This integrated approach constitutes a powerful platform for future exploration of other parameters in rationally designing optimal stimuli-responsive plasmonic hybrid sensors.

# Experimental methods

### Reagents

Gold(III) chloride trihydrate ($AuCl_3 \cdot 3H_2O$, >99.9% trace metals), ascorbic acid (AA, >99.0%), *N*,*N*′-methylenebisacrylamide (BAAm, 99%) and *N*-isopropylmethacrylamide (NIPMAm, 97%) were purchased from Sigma-Aldrich. Silver nitrate ($AgNO_3$, >99.9995% trace metals) was purchased from Strem. Hexadecyltrimethylammonium bromide (CTAB, >98.0%) and sodium oleate (NaOL, >97.0%) were purchased from TCI. Sodium borohydride ($NaBH_4$, >99%) was purchased from Honeywell Fluka. 2,2′-Azobis(2-methylpropionamidine) dihydrochloride (AAPH, 98%) was purchased from Acros. Hydrochloric acid (HCl, ACS grade), nitric acid ($HNO_3$, ACS grade), and ethanol (>99.5%) were purchased from Fisher Chemical. *N*,*N*′-Bis(acryloyl)cystamine (BAC, 98%) and phosphotungstic acid hydrate (PTA) were purchased from Alfa Aesar. All chemicals were used as received.

### Gold nanorod synthesis

All glassware was cleaned in aqua regia (1 : 3 mixture of nitric acid and hydrochloric acid) prior to synthesis. Gold nanorods were synthesized in a solution of hexadecyltrimethylammonium bromide (CTAB) and sodium oleate (NaOL) by reduction of gold(III) chloride with sodium borohydride, as previously reported.[27] Particle size and morphology were reviewed by transmission electron microscopy on a Phillips CM 12 (120 kV). Particle sizes were analyzed using the image analysis software package FIJI.[42] UV-Vis spectroscopy was performed with a Hitachi Dual Beam U3100 equipped with a temperature-controlled cuvette holder (Quantum Northwest TC100). Spectra were acquired from 700 to 1000 nm with a 5 nm slit width and 120 nm minute$^{-1}$ scan speed. Temperature was increased by 1 °C min$^{-1}$ and a spectrum was acquired once every 3 minutes.

### Refractive index dependence

The dependence of the AuNR plasmon resonance on refractive index was determined for each batch of AuNRs. The nanorods were dissolved in varying concentrations (0–100%) of glycerol in $ddH_2O$ and the absorbance spectrum of the AuNRs was taken. The peak wavelength of the longitudinal plasmon resonance was determined and plotted *versus* refractive index (as calculated by the weighted average of water and glycerol according to the concentration) in order to determine the shift in the plasmon per refractive index unit.

### Hydrogel bead synthesis

PNIPMAm beads were synthesized as previously reported.[21,28,43] First, CTAB and NaOL surfactants were partially replaced by the polymerizable ligand BAC. AuNRs were collected by centrifugation at 4300 r.c.f. for 1 hour and resuspended in 90 mL $ddH_2O$. Ethanol (10 mL) and BAC (40 mg) were added and the sample was stirred overnight. The ligand-exchanged AuNRs were then again collected by centrifugation at 4300 r.c.f. for 1 hour and resuspended in 15.0 mL $ddH_2O$.

Encapsulation of gold nanorods into PNIPMAm beads crosslinked with *N*,*N*′-methylenebisacrylamide in a 10 : 1 weight ratio was performed by batch polymerization. NIPMAAm (0.100 g) and BAAm (0.010 g) were dissolved in 15.0 mL $ddH_2O$ and heated to 70 °C under nitrogen. Ligand-exchanged AuNRs (2.0 mL) were injected, followed by 80 μL 100 mM AAPH one minute later. The reaction was stirred at 70 °C for 2 hours, during which the solution acquired a cloudy appearance indicating the growth of the collapsed hydrogel. The newly formed AuNR@PNIPMAm were cooled to room temperature and cleaned by centrifugation at 4300 r.c.f. for 1 hour and resuspension in

ultrapure water. Samples were stained by phosphotungstic acid for imaging in transmission electron microscopy.

### Nuclear magnetic resonance

$^1$H NMR measurements were performed on a Bruker Avance III 400 MHz NMR equipped with a gradient $Z$ coil and temperature control. The temperature was calibrated using a methanol-d4 external standard, and the gradient was calibrated using the diffusion of water in $D_2O$. DOSY was performed with the pulse program ledbpgp2s, with a 100 ms diffusion time and 1.4 ms gradient pulse. The diffusion constant was determined from the integrated areas *versus* gradient strength by a least-squares fit to the function:

$$I = I_0\, e^{-D\gamma^2 g^2 \delta^2 \left(\Delta - \frac{\delta}{3}\right)}$$

where $I$ is the integrated intensity, $I_0$ is the integrated intensity at gradient = 0, $D$ is the diffusion constant, $\gamma$ is the gyromagnetic ratio of the nucleus, $g$ is the gradient strength, $\delta$ is the gradient duration and $\Delta$ is the diffusion time.

T1 measurements were performed with the pulse program t1ir and delay times between 0.001 and 15 seconds. The inversion recovery time was determined by a least-squares fit to the function:

$$I = I_0 + P\, e^{-\tau/T1}$$

where $I$ is the integrated intensity, $\tau$ is the delay time, $I_0$ is the integrated intensity at infinite delay time, $P$ is the integrated intensity at $\tau = 0$, and T1 is the relaxation time.

### Dynamic light scattering

The instrument is an ALV compact goniometer system with multi-detectors (CGS-3MD, Germany) and the wavelength of He–Ne laser beam is 632.8 nm. The autocorrelation function, $g_2(\tau)$, was collected using ALV-7004 digital multiple tau real time space. The $g_2(\tau)$ can be described as an exponential decay, $e^{-2q^2Dr}$, where $D$ is the translation diffusion coefficient and $q$ is the scattering vector, $\frac{4n\pi}{\lambda}\sin\frac{\theta}{2}$, with refraction index of solution, $n$. In this experiment, the scattering angle was set at 90°. Based on the Stokes–Einstein relation, the hydrodynamic radius ($R_H$) is related to $D$ of spherical particles *via* $R_H = k_B T/6\pi\eta D$, where $k_B$ and $\eta$ are the Boltzmann constant and the solvent viscosity, respectively. The plot of $R_H$ distribution was based on intensity-weighed outcomes. The temperatures were controlled at 25, 35, 45, 47, 49, 51, 55, 60 °C in water bath.

### Small angle X-ray scattering (SAXS)

SAXS experiments were conducted by using the 16ID-LiX Beamline at the National Synchrotron Light Source II where is located at the Brookhaven National Laboratory (Upton, NY). The AuNR@PNIPMAm solutions were loaded in a sample cell sandwiched by two mica windows with a gap of ~2 mm and a window area of 18 mm$^2$ to allow the beam passing through. All samples were heated and cooled in sequence: 25, 35, 45, 47, 49, 51, 55, 60, 51, 45, 35 and 25 °C. The X-ray energy was 13.5 keV. The sample-to-detector distance is ~3 m and the exposure time is 1 second. The intensity is expressed as a function of scattering vector, $q$ defined as $\frac{4\pi}{\lambda}\sin\frac{\theta}{2}$, where $\theta$ is the scattering angle, and $\lambda$ is the wavelength. The data over a $q$ range from 0.005 to 2.5 Å$^{-1}$. Radial averaging and $q$-conversion of data were analyzed by using Jupyter Notebook. The background subtraction and transmission correction were performed to minimize the intensity of the hydrogen bond from water at ~2.0 Å$^{-1}$.

## Abbreviations

| | |
|---|---|
| AuNR | Gold nanorod |
| DLS | Dynamic light scattering |
| NMR | Nuclear magnetic resonance |
| PNIPMAm | Poly(*N*-isopropylmethacrylamide) |
| SAXS | Small angle X-ray scattering |
| TEM | Transmission electron microscopy |

## Author contributions

Conceptualization and supervision: M. P. N. and L. A. H. Data curation, formal analysis, and visualization: K. Z., C. H. L., E. R. B., H. A. and L. A. H. Investigation: K. Z., C. H. L., E. R. B., H. A. Writing – original draft: L. A. H. Writing – review & editing: all authors.

## Conflicts of interest

There are no conflicts to declare.

## Acknowledgements

The authors would like to thank Dr Lin Yang and the beamtime of 16ID-LiX at the NSLS-II (Brookhaven National Laboratory) through a beamtime proposal (BAG-302208). The LiX beamline is part of the Center for BioMolecular Structure (CBMS), which is primarily supported by the National Institutes of Health, National Institute of General Medical Sciences (NIGMS) through a P30 Grant (P30GM133893), and by the DOE Office of Biological and Environmental Research (KP1605010). LiX also received additional support from NIH Grant S10 OD012331. As part of NSLS-II, a national user facility at Brookhaven National Laboratory, work performed at the CBMS is supported in part by the U.S. Department of Energy, Office of Science, Office of Basic Energy Sciences Program under contract number DE-SC0012704. The Bruker Avance III used for NMR measurements was obtained with a National Science Foundation MRI grant (NSF-MRI CHE-0619275).

## References

1 R. T. Shafranek, S. C. Millik, P. T. Smith, C. U. Lee, A. J. Boydston and A. Nelson, Stimuli-Responsive Materials in Additive Manufacturing, *Prog. Polym. Sci.*, 2019, **93**, 36–67, DOI: 10.1016/j.progpolymsci.2019.03.002.

2 M. Molina, M. Asadian-Birjand, J. Balach, J. Bergueiro, E. Miceli and M. Calderón, Stimuli-Responsive Nanogel Composites and Their Application in Nanomedicine, *Chem. Soc. Rev.*, 2015, **44**(17), 6161–6186, DOI: 10.1039/c5cs00199d.
3 D. A. Foyt, M. D. A. Norman, T. T. L. Yu and E. Gentleman, Exploiting Advanced Hydrogel Technologies to Address Key Challenges in Regenerative Medicine, *Adv. Healthcare Mater.*, 2018, **1700939**, 1700939, DOI: 10.1002/adhm.201700939.
4 A. M. Rosales and K. S. Anseth, The Design of Reversible Hydrogels to Capture Extracellular Matrix Dynamics, *Nat. Rev. Mater.*, 2016, **1**, 1–16, DOI: 10.1038/natrevmats.2015.12.
5 E. Sato Matsuo and T. Tanaka, Kinetics of Discontinuous Volume – Phase Transition of Gels, *J. Chem. Phys.*, 1998, 1695.
6 S. Saxena, C. E. Hansen and L. A. Lyon, Microgel Mechanics in Biomaterial Design, *Acc. Chem. Res.*, 2014, **47**(8), 2426–2434, DOI: 10.1021/ar500131v.
7 C. D. Jones and L. A. Lyon, Synthesis and Characterization of Multiresponsive Core-Shell Microgels, *Macromolecules*, 2000, **33**(22), 8301–8306, DOI: 10.1021/ma001398m.
8 D. Gan and L. A. Lyon, Tunable Swelling Kinetics in Core - Shell Hydrogel Nanoparticles, *J. Am. Chem. Soc.*, 2001, **123**(31), 7511–7517, DOI: 10.1021/ja010609f.
9 S. Shi, Q. Wang, T. Wang, S. Ren, Y. Gao and N. Wang, Thermo-, pH-, and Light-Responsive Poly(N -Isopropylacrylamide- Co -Methacrylic Acid)-Au Hybrid Microgels Prepared by the in Situ Reduction Method Based on Au-Thiol Chemistry, *J. Phys. Chem. B*, 2014, **118**(25), 7177–7186, DOI: 10.1021/jp5027477.
10 T. Y. Wu, A. B. Zrimsek, S. V. Bykov, R. S. Jakubek and S. A. Asher, Hydrophobic Collapse Initiates the Poly(N -Isopropylacrylamide) Volume Phase Transition Reaction Coordinate, *J. Phys. Chem. B*, 2018, **122**(11), 3008–3014, DOI: 10.1021/acs.jpcb.8b00740.
11 H. Y. Lee, Y. Cai, S. Bi, Y. N. Liang, Y. Song and X. M. Hu, A Dual-Responsive Nanocomposite toward Climate-Adaptable Solar Modulation for Energy-Saving Smart Windows, *ACS Appl. Mater. Interfaces*, 2017, **9**(7), 6054–6063, DOI: 10.1021/acsami.6b15065.
12 T. Kanai, H. Yano, N. Kobayashi and T. Sawada, Enhancement of Thermosensitivity of Gel-Immobilized Tunable Colloidal Photonic Crystals with Anisotropic Contraction, *ACS Macro Lett.*, 2017, 1196–1200, DOI: 10.1021/acsmacrolett.7b00780.
13 M. Karg and T. Hellweg, New "Smart" Poly(NIPAM) Microgels and Nanoparticle Microgel Hybrids: Properties and Advances in Characterisation, *Curr. Opin. Colloid Interface Sci.*, 2009, **14**(6), 438–450, DOI: 10.1016/j.cocis.2009.08.002.
14 K. A. Willets and R. P. V. Duyne, Localized Surface Plasmon Resonance Spectroscopy and Sensing, *Annu. Rev. Phys. Chem.*, 2007, **58**, 267–297, DOI: 10.1146/annurev.physchem.58.032806.104607.
15 H. Chen, X. Kou, Z. Yang, W. Ni and J. Wang, Shape-and Size-Dependent Refractive Index Sensitivity of Gold Nanoparticles, *Langmuir*, 2008, **24**, 5233–5237, DOI: 10.1021/la800305j.
16 K. Gawlitza, S. T. Turner, F. Polzer, S. Wellert, M. Karg, P. Mulvaney and R. v. Klitzing, Interaction of Gold Nanoparticles with Thermoresponsive Microgels: Influence of the Cross-Linker Density on Optical Properties, *Phys. Chem. Chem. Phys.*, 2013, **15**(37), 15623–15631, DOI: 10.1039/c3cp51578h.
17 M. Karg, I. Pastoriza-Santos, J. Pérez-Juste, T. Hellweg and L. M. Liz-Marzán, Nanorod-Coated PNIPAM Microgels: Thermoresponsive Optical Properties, *Small*, 2007, **3**(7), 1222–1229, DOI: 10.1002/smll.200700078.
18 M. Karg, Y. Lu, E. Carbó-Argibay, I. Pastoriza-Santos, J. Pérez-Juste, L. M. Liz-Marzán and T. Hellweg, Multiresponsive Hybrid Colloids Based on Gold Nanorods and Poly(NIPAM-Co-Allylacetic Acid) Microgels: Temperature- and pH-Tunable Plasmon Resonance, *Langmuir*, 2009, **25**(5), 3163–3167, DOI: 10.1021/la803458j.
19 M. Das, N. Sanson, D. Fava and E. Kumacheva, Microgels Loaded with Gold Nanorods: Photothermally Triggered Volume Transitions under Physiological Conditions, *Langmuir*, 2007, **23**(1), 196–201, DOI: 10.1021/la061596s.
20 M. Das, L. Mordoukhovski and E. Kumacheva, Sequestering Gold Nanorods by Polymer Microgels, *Adv. Mater.*, 2008, **20**(12), 2371–2375, DOI: 10.1002/adma.200702860.
21 R. Contreras-Cáceres, A. Sánchez-Iglesias, M. Karg, I. Pastoriza-Santos, J. Pérez-Juste, J. Pacifico, T. Hellweg, A. Fernández-Barbero and L. M. Liz-Marzán, Encapsulation and Growth of Gold Nanoparticles in Thermoresponsive Microgels, *Adv. Mater.*, 2008, **20**(9), 1666–1670, DOI: 10.1002/adma.200800064.
22 J. Rodríguez-Fernandez, M. Fedoruk, C. Hrelescu, A. A. Lutich and J. Feldmann, Triggering the Volume Phase Transition of Core-Shell Au Nanorod-Microgel Nanocomposites with Light, *Nanotechnology*, 2011, **22**(24), 245708, DOI: 10.1088/0957-4484/22/24/245708.
23 C.-F. Lee, G.-M. Zhang, M.-P. Nieh and T.-M. Don, Morphology and Opto-Thermal Properties of the Thermo-Responsive PNIPAAm-Protected Gold Nanorods, *Polymer*, 2016, **84**, 138–147, DOI: 10.1016/j.polymer.2015.12.047.
24 G. K. Joshi, K. A. Smith, M. A. Johnson and R. Sardar, Temperature-Controlled Reversible Localized Surface Plasmon Resonance Response of Polymer-Functionalized Gold Nanoprisms in the Solid State, *J. Phys. Chem. C*, 2013, **117**(49), 26228–26237, DOI: 10.1021/jp409264w.
25 X. Dong, X. Zou, X. Liu, P. Lu, J. Yang, D. Lin, L. Zhang and L. Zha, Temperature-Tunable Plasmonic Property and SERS Activity of the Monodisperse Thermo-Responsive Composite Microgels with Core-Shell Structure Based on Gold Nanorod as Core, *Colloids Surf., A*, 2014, **452**(1), 46–50, DOI: 10.1016/j.colsurfa.2014.03.090.
26 B. W. Garner, T. Cai, S. Ghosh, Z. Hu and A. Neogi, Refractive Index Change Due to Volume-Phase Transition in Polyacrylamide Gel Nanospheres for Optoelectronics and Bio-Photonics, *Appl. Phys. Express*, 2009, **2**, 057001, DOI: 10.1143/APEX.2.057001.

27 X. Ye, Y. Gao, J. Chen, D. C. Reifsnyder, C. Zheng and C. B. Murray, Seeded Growth of Monodisperse Gold Nanorods Using Bromide-Free Surfactant Mixtures, *Nano Lett.*, 2013, **13**(5), 2163–2171, DOI: 10.1021/nl400653s.

28 F. Tang, N. Ma, X. Wang, F. He and L. Li, Hybrid Conjugated Polymer-Ag@PNIPAM Fluorescent Nanoparticles with Metal-Enhanced Fluorescence, *J. Mater. Chem.*, 2011, **21**(42), 16943, DOI: 10.1039/c1jm11395j.

29 X. Hu, Z. Tong and L. A. Lyon, Control of Poly( *N* -Isopropylacrylamide) Microgel Network Structure by Precipitation Polymerization near the Lower Critical Solution Temperature, *Langmuir*, 2011, **27**(7), 4142–4148, DOI: 10.1021/la200114s.

30 R. Pelton, Unresolved Issues in the Preparation and Characterization of Thermoresponsive Microgels, *Macromol. Symp.*, 2004, **207**(1), 57–66, DOI: 10.1002/masy.200450306.

31 J. A. Allegretto, J. M. Giussi, S. E. Moya, O. Azzaroni and M. Rafti, Synthesis and Characterization of Thermoresponsive ZIF-8@PNIPAm-Co-MAA Microgel Composites with Enhanced Performance as an Adsorption/Release Platform, *RSC Adv.*, 2020, **10**(5), 2453–2461, DOI: 10.1039/C9RA09729E.

32 E. I. Tiktopulo, V. N. Uversky, V. B. Lushchik, S. I. Klenin, V. E. Bychkova and O. B. Ptitsyn, "Domain" Coil–Globule Transition in Homopolymers, *Macromolecules*, 1995, **28**(22), 7519–7524, DOI: 10.1021/ma00126a032.

33 J. Zhao, H. Su, G. E. Vansuch, Z. Liu, K. Salaita and R. B. Dyer, Localized Nanoscale Heating Leads to Ultrafast Hydrogel Volume-Phase Transition, *ACS Nano*, 2019, **13**(1), 515–525, DOI: 10.1021/acsnano.8b07150.

34 J. Witte, P. Krause, T. Kyrey, A. M. Dahl, J. Lutzki, B. V. K. J. Schmidt, M. Ganeva, A. Koutsioubas, O. Holderer and S. Wellert, Grazing Incidence Neutron Spin Echo Study of Poly(N-Isopropylacrylamide) Brushes, *Macromolecules*, 2020, **53**(5), 1819–1830, DOI: 10.1021/acs.macromol.9b01247.

35 M. Reufer, P. Díaz-Leyva, I. Lynch and F. Scheffold, Temperature Sensitive Poly(N-Isopropyl-Acrylamide) Microgel Particles: A Light Scattering Study, *Eur. Phys. J. E*, 2009, **28**, 165–171, DOI: 10.1140/epje/i2008-10387-2.

36 M. Tagliazucchi, M. G. Blaber, G. C. Schatz, E. A. Weiss and I. Szleifer, Optical Properties of Responsive Hybrid Au@polymer Nanoparticles, *ACS Nano*, 2012, **6**(9), 8397–8406, DOI: 10.1021/nn303221y.

37 A. J. Haes, C. L. Haynes, A. D. Mcfarland, G. C. Schatz, R. P. Van Duyne and S. Zou, Plasmonic Materials for Surface-Enhanced Sensing and Spectroscopy, *MRS Bull.*, 2005, **30**, 368–375.

38 J. Witte, T. Kyrey, J. Lutzki, A. M. Dahl, J. Houston, A. Radulescu, V. Pipich, L. Stingaciu, M. Kühnhammer, M. U. Witt, R. von Klitzing, O. Holderer and S. Wellert, A Comparison of the Network Structure and Inner Dynamics of Homogeneously and Heterogeneously Crosslinked PNIPAM Microgels with High Crosslinker Content, *Soft Matter*, 2019, **15**(5), 1053–1064, DOI: 10.1039/C8SM02141D.

39 B. Sierra-Martin, J. R. Retama, M. Laurenti, A. Fernández Barbero and E. López Cabarcos, Structure and Polymer Dynamics within PNIPAM-Based Microgel Particles, *Adv. Colloid Interface Sci.*, 2014, **205**, 113–123, DOI: 10.1016/j.cis.2013.11.001.

40 W. Li, H. Chung, C. Daeffler, J. A. Johnson and R. H. Grubbs, Application of 1H DOSY for Facile Measurement of Polymer Molecular Weights, *Macromolecules*, 2012, **45**(24), 9595–9603, DOI: 10.1021/ma301666x.

41 M. Andersson and S. L. Maunu, Volume Phase Transition and Structure of Poly(N-Isopropylacrylamide) Microgels Studied with 1H-NMR Spectroscopy in D2O, *Colloid Polym. Sci.*, 2006, **285**(3), 293–303, DOI: 10.1007/s00396-006-1563-y.

42 J. Schindelin, I. Arganda-Carrera, E. Frise, V. Kaynig, M. Longair, T. Pietzsch, S. Preibisch, C. Rueden, S. Saalfeld, B. Schmid, J.-Y. Tinevez, D. J. White, V. Hartenstein, K. Eliceiri, T. Pavel and A. Cardona, Fiji – an Open Platform for Biological Image Analysis, *Nat. Methods*, 2012, **9**(7), 676–682, DOI: 10.1038/nmeth.2019.Fiji.

43 Z. Liu, Y. Liu, Y. Chang, H. R. Seyf, A. Henry, A. L. Mattheyses, K. Yehl, Y. Zhang, Z. Huang and K. Salaita, Nanoscale Optomechanical Actuators for Controlling Mechanotransduction in Living Cells, *Nat. Methods*, 2016, **13**(2), 143–146, DOI: 10.1038/nmeth.3689.